Environmental Earth Sciences (2018) 77:471
https://doi.org/10.1007/s12665-018-7631-z

ORIGINAL ARTICLE

Liquefaction behavior of dredged silty-fine sands under cyclic loading for land reclamation: laboratory experiment and numerical simulation

Jianxiu Wang[1,2,3] · Yansheng Deng[1] · Yule Shao[1] · Xiaotian Liu[1] · Bo Feng[2,4] · Linbo Wu[1] · Jie Zhou[1] · Yao Yin[1] · Na Xu[1] · Haihua Peng[2]

Received: 22 September 2017 / Accepted: 18 June 2018 / Published online: 26 June 2018

Abstract
Medium-coarse sands (CS) were dredged and exhausted in land reclamation. However, the remaining silty-fine sands (FS) were wasted. The liquefaction behavior of dredged silty-FS and the possibility of utilizing the remaining silty-FS as dredger fill source for land reclamation should be investigated. Cyclic consolidation-undrained triaxial tests were performed to investigate the liquefaction resistance of dredged silty-FS under different influencing factors. The cyclic stress ratio (CSR) of dredged silty-FS increased with the increase in initial relative density and consolidation stress ratio and decreased with the increase in silt content and consolidation stress. The CSR first decreased with the increase in clay content up to a threshold value and increased with the increase in clay content. A regression model was created to estimate the relationship between CSR and silt content, clay content, initial relative density, consolidation stress, consolidation stress ratio, and cyclic resistance ratio. Response surface methodology (RSM) was employed to investigate the mutual influence among the five independent variables. On the basis of cyclic triaxial tests, particle flow code models were introduced to investigate the microscopic internal fabric changes of dredged silty-FS and the influence of extended factors on liquefaction. The average microscopic contact force and coordination number between particles controlled the macroscopic mechanical behavior of sands. Sand liquefaction was due to the cumulative loss of coordination number under cyclic loading. The average contact force between particles was linearly decreased to 0 and the coordination number sharply decreased when the sample reached initial liquefaction. On the basis of numerical tests, CSR increased with the increase in D_{50} and vibration frequency. The influence of vibration frequency was relatively small. In addition, the CS–FS and CS–FS–CS combination layers showed greater liquefaction resistance than the FS layer. In the filling process, the interbed of FS and CS improved the liquefaction resistance of dredged silty-FS to a certain extent.

Keywords Dredged silty-fine sand · Land reclamation · Liquefaction · Cyclic triaxial test · PFC numerical simulation

Introduction

The medium-coarse sands (CS) of intertidal zone and shallow sea were dredged and exhausted for large-scale land reclamation projects along the coastal areas of China. However, the silty-fine sands (FS) were not used and wasted due to the potential liquefaction problem that aggravated the shortage of backfill materials for reclamation projects. To solve the problem, laboratory experiments were conducted to investigate the liquefaction resistance of dredged silty-FS under different influencing factors, namely silt content, clay content, initial relative density, consolidation stress and consolidation stress ratio. Physical experiments were not performed for all potential working conditions and influencing factors because they were expensive and time consuming. Particle

✉ Jianxiu Wang
wang_jianxiu@163.com

1 Department of Geotechnical Engineering, College of Civil Engineering, Tongji University, Shanghai 200092, China

2 CCCC Key Laboratory of Environment Protection & Safety in Foundation Engineering of Transportation, Guangzhou 510230, China

3 Key Laboratory of Karst Collapse Prevention, CAGS, Guilin 541004, China

4 CCCC National Research Center of Dredging Technology and Equipment Co. Ltd., Shanghai 201208, China

flow code (PFC) numerical simulations were performed to supplement the physical experiments and explain the liquefaction from the micro perspective. Numerical simulations were conducted to discuss the influence of other potential influencing factors on liquefaction.

Liquefaction is one of the disastrous forms of geotechnical failures that occurs due to the rapid accumulation of pore water pressure and reduction in effective confining stress (Rahman et al. 2014). The dynamic response and liquefaction behavior of dredged silty-FS and the possibility of utilizing silty-FS in land reclamation should be investigated. However, corresponding studies have mainly focused on clean sands or sands with a small portion of fine gravel (Ishihara 1993; Liu and Yu 1999; Xenaki and Athanasopoulos 2003; Baziar and Sharafi 2011; Monkul and Yamamuro 2011; Takch et al. 2016). Cundall and Strack (1979) first investigated the mechanical properties of granular media using a discrete element method (DEM). Subsequently, the DEM was widely used in investigating the micro-mechanism of sand liquefaction (Ishihara et al. 1975; Ng and Dobry 1994; Zhou et al. 2000, 2009; Zhou and Chi 2003; Sitharam 2003; Sitharam and Vinod 2009; Liu et al. 2007a, b). Researchers have analyzed the liquefaction mechanism, trigger conditions, and liquefaction criterion of silty sands (Bouckovalas et al. 2003; Papadopoulou and Tika 2008; Stamatopoulos 2010; Baziar and Sharafi 2011; Lee et al. 2012; Jafarian et al. 2013; Sadrekarimi 2013; Park and Kim 2013; Karim and Alam 2014; Arab et al. 2014; Dobry et al. 2015; Monkul et al. 2015; Takch et al. 2016; Huang and Wang 2016; El-Sekelly et al. 2016; Kim et al. 2016) and sand-silt mixtures (Belkhatir et al. 2011; Xenaki and Athanasopoulos 2003; Stamatopoulos et al. 2015). The effect of fine contents on liquefaction susceptibility had contradictory results. The cyclic liquefaction resistance of silty sands increased (Amini and Qi 2000), decreased (Belkhatir et al. 2010; Stamatopoulos 2010), and decreased to a certain fine content and increased (Koester 1994; Polito and Martin 2001; Xenaki and Athanasopoulos 2003; Ueng et al. 2004; Ravishankar 2006; Papadopoulou and Tika 2008; Yassine et al. 2015) with the increase in fine contents. Polito (1999) reported that the influence of mean grain size (D_{50}) on liquefaction resistance was more obvious than the gradation of materials. Yilmaz and Mollamahmutoglu (2009) assessed that graded sands with small D_{50} was susceptible to liquefaction. The sand sample with small void ratio range was susceptible to liquefaction if the D_{50} of different graded sand samples was nearly the same. Belkhatir et al. (2014) confirmed that the granulometric characteristics had a significant influence on the generation of excess pore pressure of sand-silty mixture samples. Taiba et al. (2016) reported that the shear strength linearly and logarithmically decreased with the decrease in grain sizes. The tests in the sands of Toyoura Ishihara, Ottawa, and Monterey showed a considerable increase in cyclic strength with the decrease in sand void ratio (Finn et al. 1971). The cyclic strength of similar void ratio decreased with the increase in consolidation stress. Stamatopoulos et al. (2015) investigated the effect of preloading on liquefaction cyclic strength of silty sands in the free-field condition. The test results showed an obvious increase in liquefaction cyclic strength with the increase in pre-stress ratio. These studies promoted the analysis on liquefaction susceptibility of silty sands. However, the physical–mechanical properties of dredged silty-FS were relatively different with undisturbed silty-FS under natural sedimentation conditions. First, the dredged silty-FS were artificially formed using dredging technology. Second, the dredged silty-FS experienced a short history under artificial sediment environment. Third, silty-FS were unusually used as dredger fill source when medium CS were sufficient. Few studies have investigated the liquefaction behavior of dredged silty-FS for land reclamation.

In this study, the liquefaction behavior of dredged silty-FS was investigated using cyclic triaxial tests. On the basis of test results, the effects of five independent variables on CSR were evaluated. The microscopic liquefaction behavior and extended influencing factors of dredged silty-FS were analyzed using the PFC model. Countermeasures were suggested to improve the CSR of dredged silty-FS. This study can be used as a reference for land reclamations with sufficient silty-FS and insufficient medium-CS sources.

Background

The eastern economic zone of Shantou City includes Xinjin, Xinxi, and Tagangwei areas. The economic zone is 12.5 km long with a planning area of 24.35 km^2, which is from the Bay Bridge in the west to Chenghailaiwu in the east (Fig. 1). Infrastructure construction, which includes the major and subordinate roads of these areas, is significant for the development of the eastern economic zone. On the basis of previous exploration data, the saturated sands within 20 m of the field include dredged silty-FS (layer ①), FS (layer $①_1$), and medium FS (layer ③). Dredged silty-FS are loose and saturated with an average thickness of 7 m. Dredged silty-FS have severe liquefaction layers with an average liquefaction index of 19.09. FS have medium liquefaction layers with an average liquefaction index of 15.79. Medium FS have mild to medium liquefaction layers with an average thickness of 2.5 m and their average liquefaction index is 4.27. Therefore, secondary disasters caused by liquefaction in engineering construction should be considered. The liquefaction behavior of dredged silty-FS should be investigated by using cyclic triaxial tests and numerical simulation method, and the countermeasures for land reclamation should be proposed.

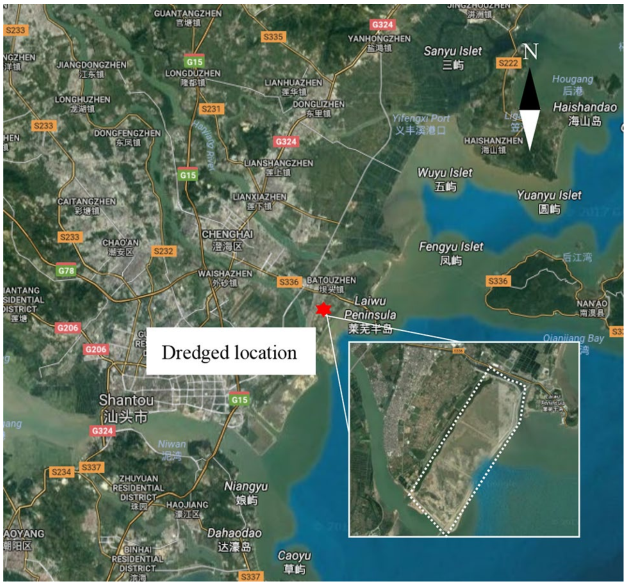

Fig. 1 Dredged location of Tagang Area, Shekou, China

Laboratory experiment

Materials and methods

Cyclic triaxial tests were performed to simulate the dynamic response of dredged silty-FS. The dredged specimens were collected from Tagangwei Eastern Economic Zone of Shantou City, Guangdong Province, China. The grain size distributions of dredged materials are presented in Fig. 2. The specimens were pretreated by drying. The grain sieves with a size of 0.075–0.25 mm were used as sands. The grains finer than 0.075 mm were used as silt, and clay particles were prepared by kaolin. Silty-FS were boiled and cooled before the test. The clay particles were added and stirred in the pulp after soaking with vacuum exhaust. The mixture was layered into a split mold tied in a latex film, and the split mold was removed under negative pressure. The maximum and minimum dry densities of the samples were 1.62 and 1.30 g/cm^3, respectively. The maximum and minimum void ratios were 1.077 and 0.667, respectively.

A GDS dynamic triaxial apparatus was adopted in the tests (Fig. 3). The dimensions of the samples were 39.1 mm in diameter and 80 mm in height. The samples were first saturated with percolating carbon dioxide through the specimen for 30 min followed by the application of de-aired water. Back pressure was applied to complete the saturation for 120 min. The minimum *B* value obtained for the tests was 0.95. A frequency of 1.0 Hz was maintained in the entire test program. An initial liquefaction criterion (Seed and Lee 1966) was adopted in the failure criterion of isotropic consolidation. Liquefaction occurred ($\Delta u/\sigma_c' = 1$) when the pore pressure exceeded the initial effective confining pressure. Experience has shown that coarse-grained sands or sands with few clay contents were easy to liquefy completely. However, the monitored excess pore pressure was small although the deformation was large for fine-grained sands with high clay content. A deformation criterion was adopted in the failure criterion of anisotropic consolidation for all cases. The corresponding value of double amplitude strain was 5% ($\varepsilon_f = 5\%$).

The influences of silt content, clay content, initial relative density, consolidation stress, and consolidation stress ratio on the liquefaction of dredged silty-FS were discussed in five working conditions (Table 1).

Liquefaction behavior observed in cyclic triaxial tests

Five series of stress-controlled cyclic triaxial tests were conducted on dredged silty-FS samples with different silt content (f_s), clay content (f_c), initial relative density (f_{ird}),

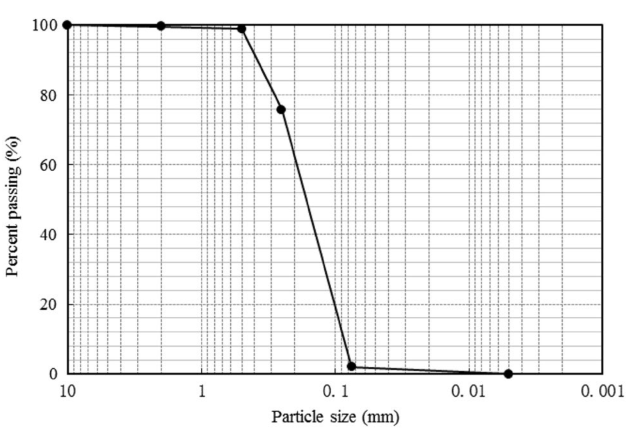

Fig. 2 Grain size distribution of dredged materials

Fig. 3 GDS test equipment

Table 1 Cyclic triaxial test design

Conditions	Silt content (%)	Clay content (%)	Initial relative density (%)	Consolidation stress (kPa)	Consolidation stress ratio
1	0	0	72	100	1
2	3	0	72	100	1
3	6	0	72	100	1
4	9	0	72	100	1
5	12	0	72	100	1
6	15	0	72	100	1
7	18	0	72	100	1
8	0	3	52	100	1
9	0	6	52	100	1
10	0	9	52	100	1
11	0	12	52	100	1
12	0	15	52	100	1
13	18	0	52	100	1
14	18	0	72	100	1
15	18	0	92	100	1
16	18	0	52	50	1
17	18	0	52	100	1
18	18	0	52	200	1
19	18	0	52	300	1
20	18	0	52	100	1
21	18	0	52	116.5	1.3
22	18	0	52	113.5	1.7
23	18	0	52	150	2.0

consolidation stress (f_{cs}), and consolidation stress ratio (f_{csr}) under undrained conditions to simulate the undrained field behavior during earthquakes. Other constants were maintained with the change of one parameter to investigate the influence on liquefaction resistance characteristics. The variation of CSR (CSR $= \sigma_d / 2\sigma'_c$) with the required number of cycles N for liquefaction is shown in Fig. 4. For a given number of cycles, CSR decreased with the increase of f_s from 0 to 18% (Fig. 4a). CSR sharply decreased (approximately 22%) when f_s value was greater than 6%. A limited percentage of silt in dredged silty-FS decreased the liquefaction resistance obviously. Silt should be separated from FS in the dredging process. The effect of f_c on CSR is shown in Fig. 4b. For a given number of cycles, CSR initially decreased with the increase on f_c up to a threshold value of 12% and increased with the increase on f_c. The effect of f_{ird} on CSR is shown in Fig. 4c. CSR increased by approximately 25% with the increase of f_{ird} from 52 to 92%. The effect of f_{ird} on CSR was not obvious. The liquefaction resistance was improved by improving f_{ird} using convenient and economic foundation treatments, such as dynamic compaction and vibroflotation. The variation of CSR with f_{cs} is shown in Fig. 4d. For a given number of cycles, CSR decreased with the increase of f_{cs} from 50 to 300 kPa. In addition, the effect of the increase on f_{cs} gradually decreased. Few changes were observed in CSR when $f_{cs} > 200$ kPa. The liquefaction resistance of dredged silty-FS was improved using preloading or overload methods. On the contrary, CSR increased with the increase of f_{csr} from 1 to 2 (Fig. 4e). According to Wang and Zhou (2001), CSR increased with the increase of f_{csr} and decreased when f_{csr} increased to threshold k_c, which can be described as

$$k_c = \frac{1 + \sin\phi}{1 - \sin\phi}, \quad (1)$$

where φ is the initial dilatancy angle.

In this way, many tests and future studies should be conducted for k_c with different f_{csr}.

Influence factor analysis for liquefaction behavior

The cyclic resistance ratio, CRR_{30}, is defined as the CSR that causes liquefaction at 30 cycles of loading. On the basis of the cyclic triaxial test results (Fig. 4), the variation of CRR_{30} with different influencing factors is shown in Fig. 5. CRR_{30} increased with the increase of f_{ird} and f_{csr} (positive effect) and decreased with the increase of f_s and f_{cs} (negative effect) (Fig. 5). CRR_{30} initially decreased and reached the minimum value at a threshold of clay content ($f_c = 12\%$) and increased with the increase of f_c. According to Thevayanagam and Martin (2002), the presence of fines (silt and clay contents in this study) reduced the liquefaction resistance of soil samples up to the threshold value and sharply increased. The distributed fines among the voids contacted coarse particles when fine content was less than the threshold value. The fines did not significantly influence the mechanical behavior of soil samples. The fines caused the instability and compressibility of the structure that resulted in the decrease of resistance. The mechanical behavior of soil samples was dominated by fine contacts when the fine content was more than the threshold value (Lade and Yamamuro 1997). This condition indicated that fines had a positive contribution and increased the soil resistance to liquefaction. Therefore, a possible critical value for silt content was observed in which the cyclic resistance sharply increased.

As shown in the range of Fig. 5, the effect of single factor on CRR_{30} is shown in Fig. 6. The difference of CRR_{30}, $\Delta_{CRR30} = 0.17$, had the most obvious effect on CRR_{30} when f_s varied from 0 to 18%. f_{cs} had the second obvious effect. $\Delta_{CRR30} = 0.07$ when f_{cs} increased from 50 to 300 kPa. f_c and f_{ird} had an equal effect due to equal Δ_{CRR30}. f_{csr} had a minimal impact on CRR_{30}. $\Delta_{CRR30} = 0.04$ when f_{csr} varied from 1 to 2. The effect of single factor was sorted as $f_s > f_{cs} > f_c$ and $f_{ird} > f_{csr}$.

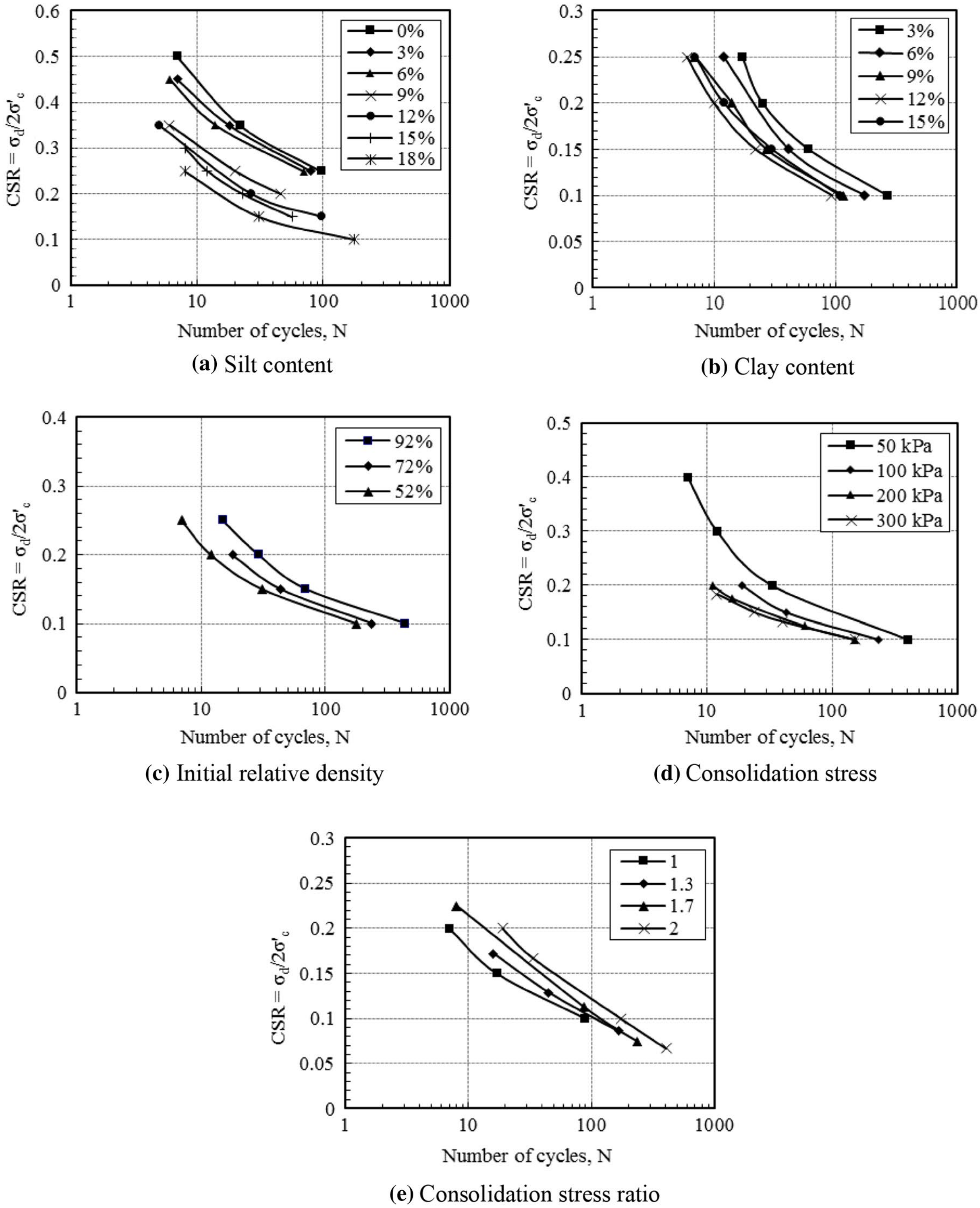

Fig. 4 Variation of CSR, $\sigma_d/2\sigma'_c$, with number of cycles, N

Regression analysis on liquefaction behavior

A regression analysis was performed to investigate the mutual-influence law among the five influencing factors. The five influencing factors were determined as five independent variables in the regression analysis. The values of five independent variables were determined through the results of cyclic triaxial tests. Equation (2) shows the relationship between CRR_{30} and f_s, f_{cs}, f_c, f_{ird}, and f_{csr}:

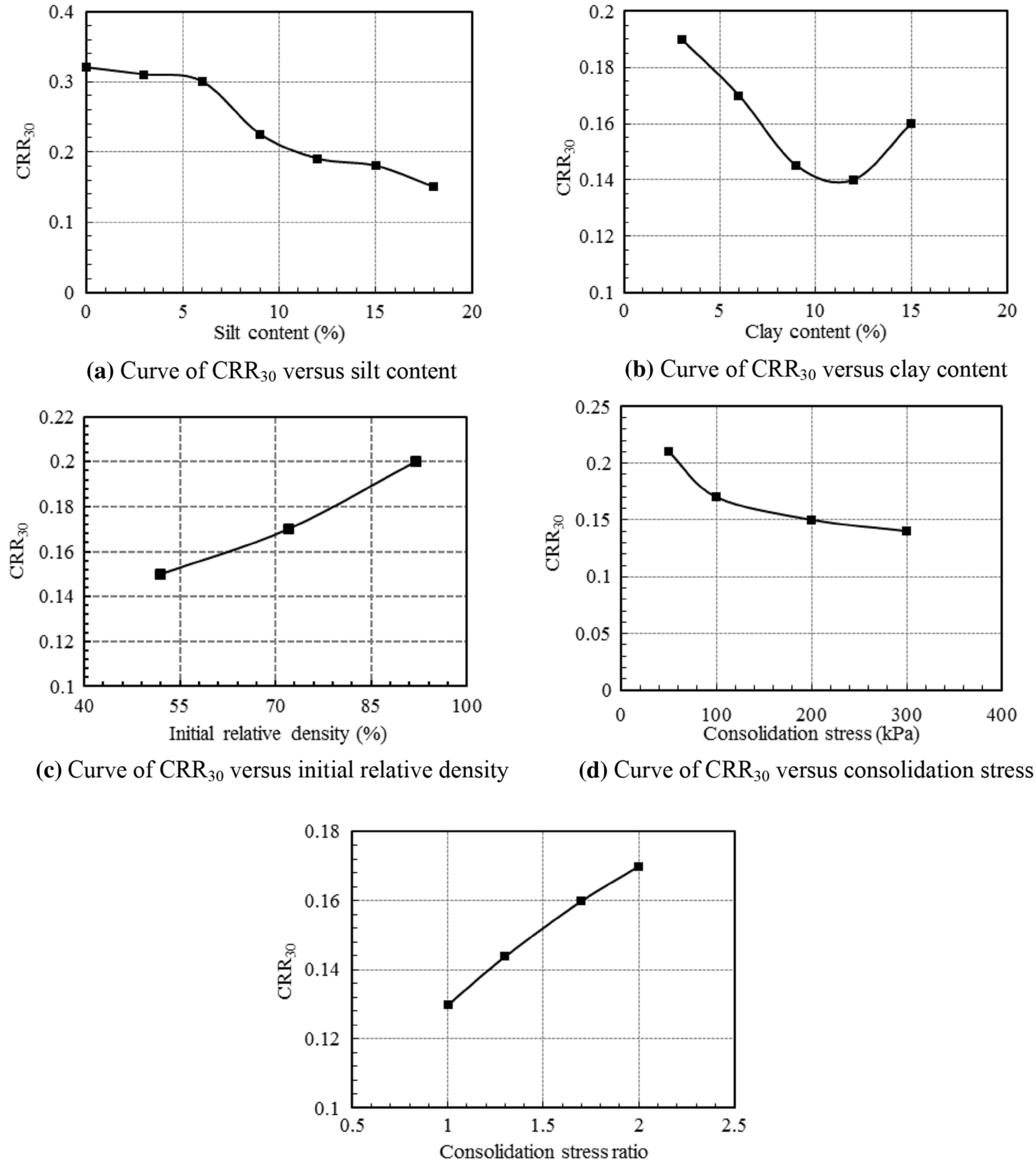

(a) Curve of CRR_{30} versus silt content

(b) Curve of CRR_{30} versus clay content

(c) Curve of CRR_{30} versus initial relative density

(d) Curve of CRR_{30} versus consolidation stress

(e) Curve of CRR_{30} versus consolidation stress ratio

Fig. 5 Variation of cyclic resistance ratio, CRR_{30}, with various parameters

$$Y = 0.125 \times 10^{-4} \times X_1^{-0.217} \times X_2^{0.073}(-0.051 \times X_3 + 1.89) \times (0.043 \times X_4^2 - 0.893 \times X_4 + 7.83) \times (-0.586 \times X_5^2 + 74.29 \times X_5 + 2363.895), \tag{2}$$

where Y is CRR_{30}. X_1, X_2, X_3, X_4, and X_5 are f_{cs} (kPa), f_{csr}, f_s (%), f_c (%), and f_{ird} (%), respectively.

The test results and regression model are shown in Fig. 7a. The regression model estimated the relationship between the variables and CRR_{30}. Most of the data of the regression model were within ± 10% of the test results (Fig. 7b). The root mean square was $R^2 = 0.883$. The regression model was used to represent the complex relationship between the five independent variables and CRR_{30}.

3D response surface plots (Fig. 8) were introduced to illustrate the relationship between CRR_{30} and experimental variables. These plots presented the functional response of two factors and maintained other variables constant at

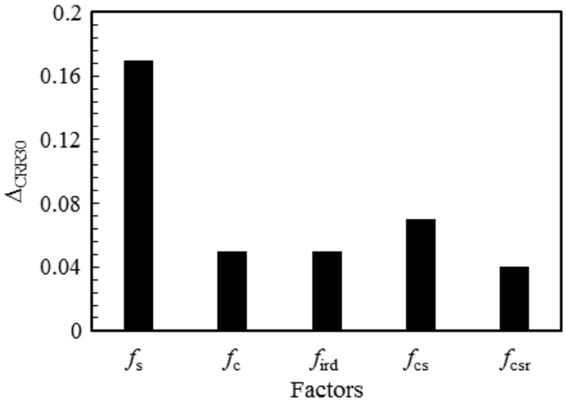

Fig. 6 Effect of different single factors on CRR30

their middle value. As shown in Fig. 8a, a large CRR_{30} was yielded when f_s was 0–3% and f_c was 3–6%. CRR_{30} gradually decreased with the increase of f_s and f_c. CRR_{30} increased with the increase of f_c when f_c achieved the threshold value (approximately 12%). The effects of f_s and f_{ird} on CRR_{30} are shown in Fig. 8b. A large CRR_{30} was obtained when f_s was 0–3% and f_c was 50–80%. The relationship of f_s and f_{cs} with CRR_{30} is shown in Fig. 8c. CRR_{30} gradually increased with the decrease of f_s and f_{cs}. CRR_{30} sharply increased when f_s was 0–3% and f_{cs} was 50–100 kPa. The relationship of f_s and f_{cs} on CRR_{30} was represented as a plane curve (Fig. 8d). f_s and f_{cs} had monotonic influences on CRR_{30}. The effect of f_c and f_{ird} on CRR_{30} was denoted as a saddled shape (Fig. 8e). A large CRR_{30} was obtained when f_c was 3–5% and f_{ird} was 60–70 kPa, which was similar to the effect of f_c and f_{csr} on CRR_{30} (Fig. 8g) at f_{csr}. A larger CRR_{30} was obtained when f_c was 3–5% and f_{cs} was 50–100 kPa (Fig. 8f). CRR_{30} gradually increased with the decrease of f_{ird} and f_{cs} and reached a large value at approximately 60% and 50 kPa (Fig. 8h). The relationship of f_{ird} and f_{csr} on CRR_{30} is shown in Fig. 8i. CRR_{30} gradually increased with the decrease of f_{ird} and increase of f_{cs} and achieved a large value at approximately 60% and 2.

Numerical experiment

On the basis of laboratory experiments, numerical models were developed for numerical experiments to analyze the dynamic response and liquefaction mechanism of dredged silty-FS. PFC was employed to simulate the liquefaction behavior from a micro-scale after calibration using the laboratory experiments. The laboratory experiments were reproduced and extended to investigate other working conditions that were not performed in the physical experiments. The microscopic internal fabric changes of dredged silty-FS and extended influencing factors for liquefaction that were not considered in the physical experiments were investigated. Meanwhile, combined countermeasures to improve liquefaction resistance were simulated and verified using the calibrated numerical models.

PFC model

Dredged silty-FS belong to granular materials, and the characteristics and contact model for particles must be properly considered in a numerical modeling. PFC 3D (PFC^{3D}) developed by Itasca was applied in this study to employ the linear contact model for simulating the mechanical behavior of particles. PFC^{3D} was able to simulate complex loading tests that were difficult to conduct experimentally and enabled the access to information at the particle level. The microscopic behavior at particle scale was investigated.

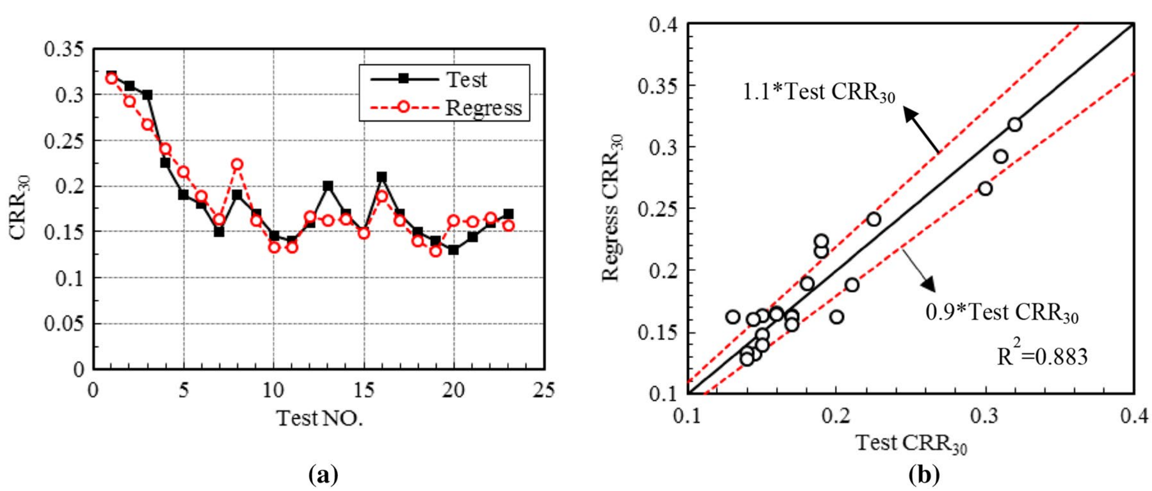

Fig. 7 Results of tests and regression

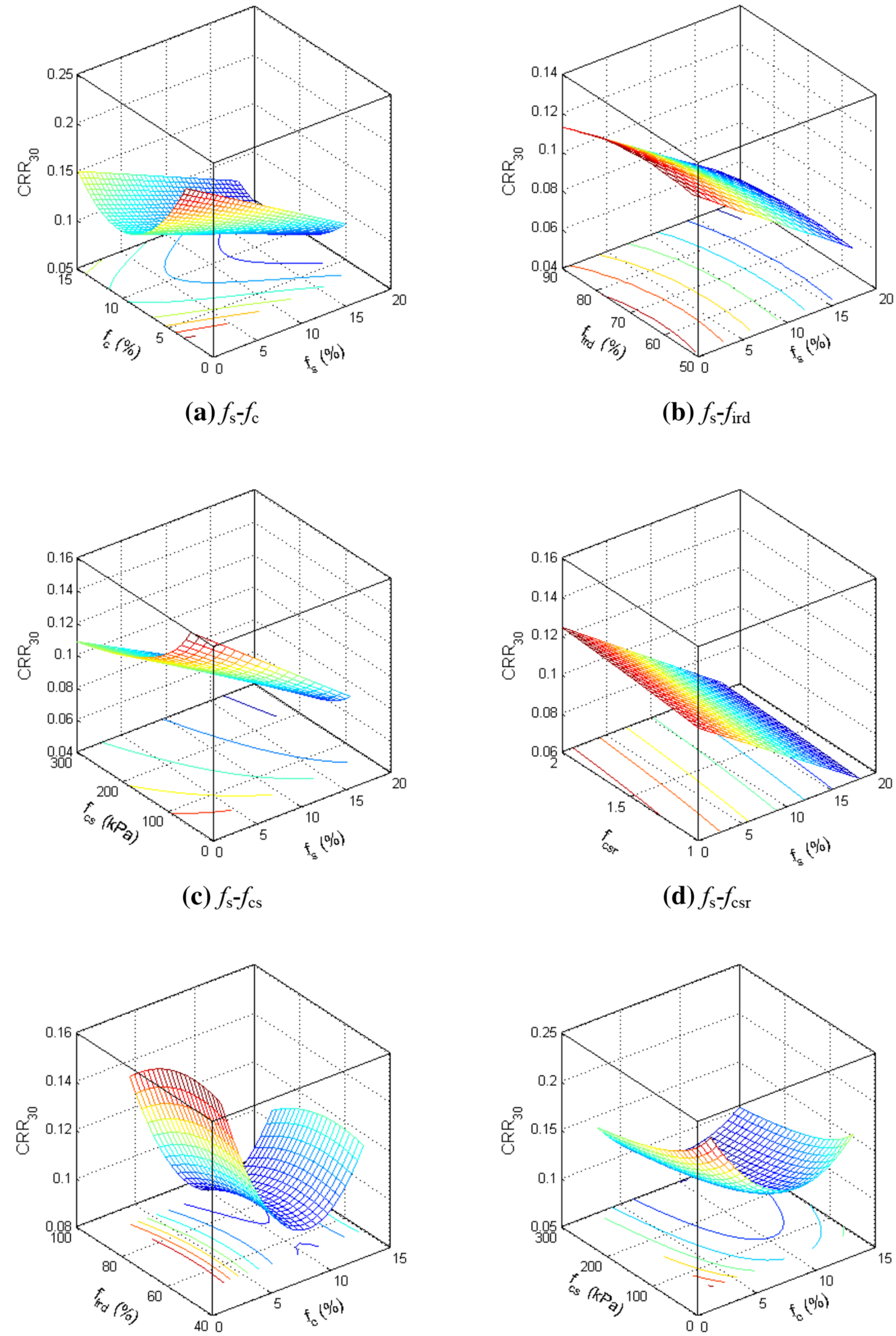

(a) f_s-f_c (b) f_s-f_{ird}

(c) f_s-f_{cs} (d) f_s-f_{csr}

(e) f_c-f_{ird} (f) f_c-f_{cs}

Fig. 8 Response surface plots for the effect of different parameters on CRR_{30}

Numerical servo-mechanism of confined pressure.

In the consolidated simulation, the top and bottom walls of the specimen were used to simulate the loading face, and the surrounding walls were used to simulate the surrounding pressure. The top and bottom faces exerted a load on the specimen under certain velocity. The lateral velocity of surrounding walls was adjusted to exert a constant confined pressure on the specimen. A numerical servo-mechanism was adopted to automatically control the velocity of surrounding walls.

The velocity of surrounding wall is expressed as

Fig. 8 (continued)

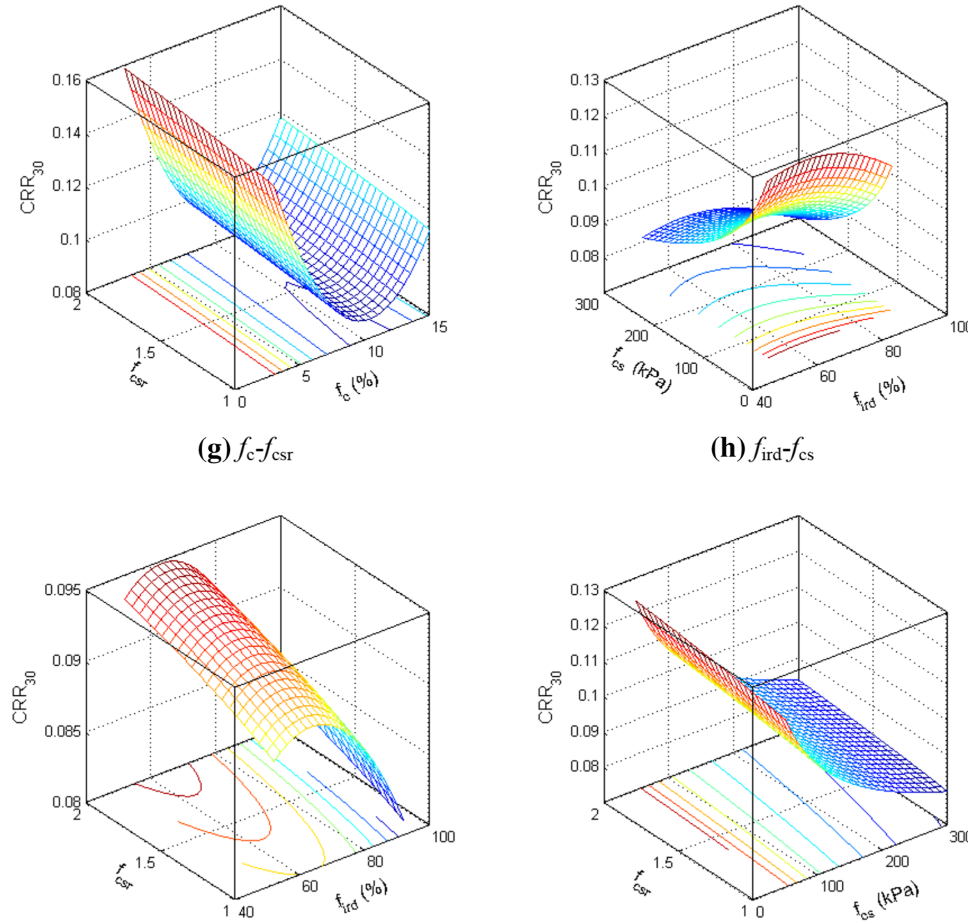

(g) f_c-f_{csr} **(h)** f_{ird}-f_{cs}

(i) f_{ird}–f_{csr} **(j)** f_{cs}–f_{csr}

$$\dot{\mu}^{(\omega)} = G(\sigma_m - \sigma_t) = G\Delta\sigma, \tag{3}$$

where G is the coefficient to determine the velocity of the surrounding wall, σ_m is the monitored confined pressure (kPa), and σ_t is the exerted confined pressure (kPa).

In one calculation time step, the maximum force increment induced by wall movement is expressed as

$$\Delta F^{(\omega)} = k_n^{(\omega)} N_c \dot{\mu}^{(\omega)} \Delta t, \tag{4}$$

where N_c is the contact number of particles with the wall, and k_n^{ω} is the average contact stiffness (kN/m).

The average increment of force on the walls is expressed as

$$\Delta\sigma^{(\omega)} = \frac{k_n^{(\omega)} N_c \dot{\mu}^{(\omega)} \Delta t}{A}, \tag{5}$$

where A is the area of the walls (m^2).

To maintain the stability of calculation, the absolute value of wall stress variation must be less than the absolute value on the difference between the pre-exerting wall and actual stresses. Safe coefficient α is introduced to maintain the stability

$$\Delta\sigma^{(\omega)} < \alpha|\Delta\sigma|. \tag{6}$$

Equations (2) and (3) are substituted to Eq. (4) to obtain

$$\frac{k_n^{(\omega)} N_C G|\Delta\sigma|\Delta t}{A} < \alpha|\Delta\sigma|. \tag{7}$$

G can be obtained through Eq. (5)

$$G = \frac{\alpha A}{k_n^{\omega} N_C \Delta t,} \tag{8}$$

here α was adopted as 0.5.

Sinusoidal cyclic load

A sub-program of FISH language was developed to simulate the sinusoidal load. The sinusoidal load was realized using the numerical servo-mechanism. The sinusoidal load was transferred to velocity and exerted on the surrounding walls. The velocity was adjusted in real time by comparing the stress errors.

Pore pressure

The undrained condition was realized by constant volume conditions during the loading course. We suppose the initial height of the specimen was h and the initial diameter was r. The velocity of the top and bottom walls was v_z, and the velocity of the surrounding wall was v_r during the loading procedure. The volumetric strain is expressed as

$$\varepsilon_v = \varepsilon_z + \varepsilon_r, \tag{9}$$

where $\varepsilon_v = 0$,

$$v_r = \frac{-\left((r\sqrt{h(h-2v_z t)} - hr + 2rv_z t\right)}{-2v_z t^2 + ht}. \tag{10}$$

Under constant volume condition, the variation of pore pressure induced by cyclic loading was obtained by monitoring the variation of effective stress on the surrounding wall

$$u = \sigma'_{30} - \sigma'_3, \tag{11}$$

where σ'_{30} is the initial effective lateral confining pressure (kPa), and σ'_3 is the effective axial stress (kPa).

Microscopic parameter calibration

A set of representative cyclic triaxial tests for dredged silty-FS was selected to calibrate the microscopic parameters based on PFC^{3D}. The numerical triaxial specimen was 3.91 cm in diameter and 8 cm in height based on the cyclic triaxial tests. According to Zhou et al. (2009), the appropriate enlargement of average particle size did not affect the macroscopic mechanical properties of the sample when the calculated particle number exceeded 2000 based on DEM (Zhou et al. 2009). The diameter of particles ranged from 1.2 to 2.4 mm, and a uniform distribution was adopted. The total number of particles used in the simulation was 2351 (Fig. 9). A linear stiffness model was introduced to simulate the stiffness characteristics of dredged silty-FS. A trial-and-error method was employed to calibrate the microscopic parameters.

To accurately calibrate the microscopic parameters, a sinusoidal curve with variable amplitude was used as the cyclic load of the PFC^{3D} model (Fig. 10). Under constant volume conditions, the pore pressure was monitored by the variation of lateral effective confining pressure. The deviator stress (q'), effective mean principal stress (p'), deviator strain (ε), and excess pore pressure (u) are expressed as

$$\begin{cases} q' = \frac{\sigma'_1 - \sigma'_3}{2}; \quad p' = \frac{\sigma'_1 + \sigma'_3}{2} \\ \varepsilon = \varepsilon_1 - \varepsilon_3; \; u = \sigma'_{30} - \sigma'_3 \end{cases}, \tag{12}$$

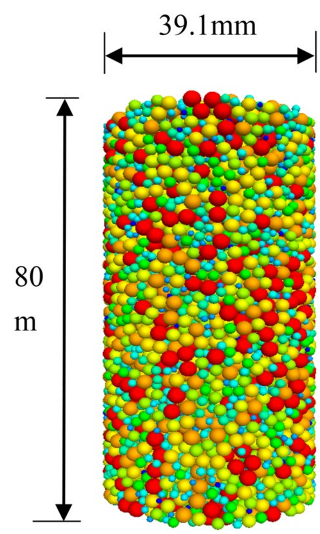

Fig. 9 PFC numerical sample

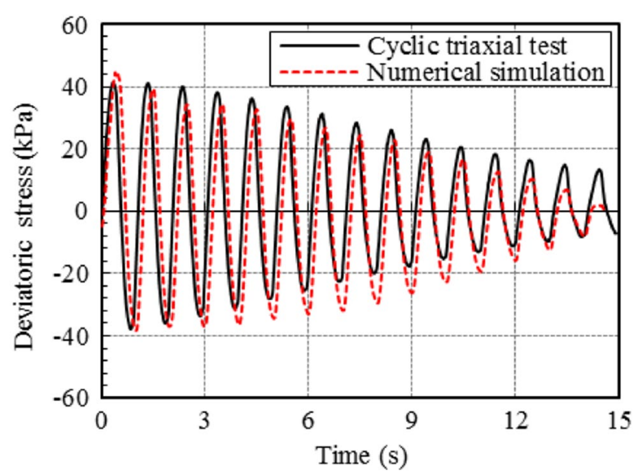

Fig. 10 Deviatoric stress curves of test and numerical simulation

where σ'_1 and σ'_3 are the effective axial and lateral stresses (kPa); ε'_1 and ε'_3 are the effective axial and lateral strains, respectively; and σ'_{30} is initial effective lateral confining pressure (kPa).

The excess pore water pressure–time curves of cyclic triaxial test and numerical simulation are shown in Fig. 11. The excess pore water pressure increased with the increase of cyclic number. The effective mean principal stress gradually decreased with the decrease of deviator stress and increase of excess pore pressure (Fig. 12). The numerical simulation results agreed well with the cyclic triaxial test (Figs. 11, 12). The microscopic parameters are calibrated in Table 2.

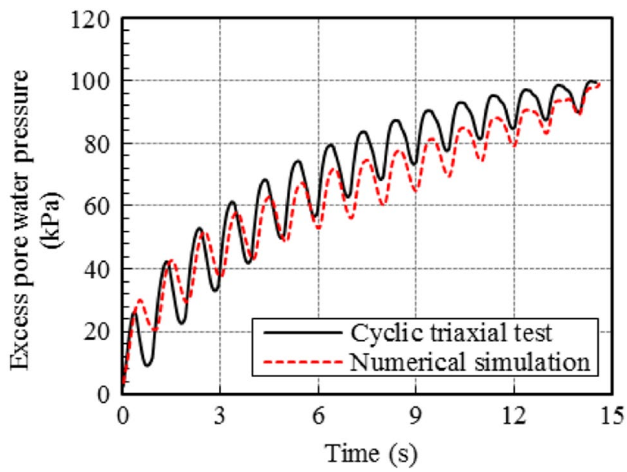

Fig. 11 Excess pore water pressure curves between cyclic triaxial test and numerical simulation

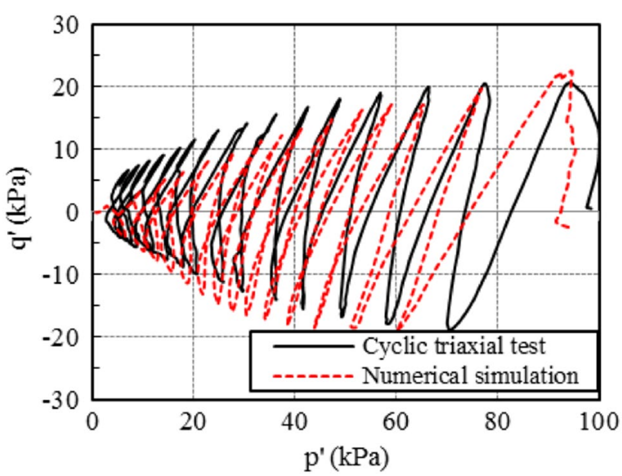

Fig. 12 $p' - q'$ curves of cyclic triaxial test and numerical simulation

Table 2 Model parameters used in PFC simulations

Parameters	k_n (N/m)	k_s (N/m)	μ	ρ (kg/m^3)
Value	7×10^6	7×10^6	0.5	1520

Internal fabric change in the liquefaction process

The PFC^{3D} numerical simulation obtained the macroscopic response of liquefaction and also the internal fabric changes on liquefaction. The average contact force (X-, Y-, and Z-directions) and coordination number were monitored to investigate the internal fabric changes in the liquefaction process. The average contact force in the X-, Y-, and Z-directions and excess pore water pressure curves based on the numerical model are shown in Fig. 13. The average contact force in the X and Y directions linearly decreased with the increase of excess pore water pressure. However, the average contact force cyclically decreased in the Z-direction that was similar to deviator stress. The average contact force in the X-, Y-, and Z-directions decreased to 0 kPa when the excess pore water pressure increased to the initial effective lateral confining stress (100 kPa), which implied that the initial liquefaction condition was achieved.

N' was defined as the cyclic times when initial liquefaction was achieved. The cyclic vibration times (N/N')-coordination number curve is shown in Fig. 14. The coordination number slightly decreased at the start ($N/N' < 0.15$) and was kept steady. The coordination number rapidly diminished to 2.75 when $N/N' > 0.6$. Simultaneously, the excess pore water pressure increased to 100 kPa. The particles were in suspension state and local macroscopic liquefaction occurred when the average contact force decreased to 0 kPa, which was also indicated by contact force chain between the particles of the numerical sample. The change of contact force chain between the particles before and after liquefaction is shown in Fig. 15. The contact force chain intensely dropped after liquefaction.

Influences of D_{50} and vibration frequency based on PFC

D_{50} and vibration frequency were not considered in the cyclic triaxial tests. However, their influence on CSR was discussed based on the numerical models. The microscopic parameters of dredged silty-FS and the influences of D_{50} (0.35, 0.65, 0.75, and 0.85 mm) and vibration frequency (1, 2, 3, and 4 Hz) on liquefaction were investigated using numerical tests to compensate for insufficient experiments. The consolidation stress was 100 kPa. All of the numerical models followed a uniform distribution. The linear contact model was adopted for all particles from the start of generation.

The effect of different D_{50} on CSR is shown in Fig. 16. CSR increased with the increase of D_{50}. CSR slowly increased when $D_{50} > 0.75$ mm. CSR increased by 86% when D_{50} increased from 0.35 to 0.65 mm. CSR increased by 4.7% when D_{50} increased from 0.75 to 0.85 mm. This finding was similar to the test results that for any two differently graded grains of sand, the grains that had a smaller D_{50} were more susceptible to liquefaction (Yilmaz and Mollamahmutoglu 2009). On this basis, the possibility of dredged silty-FS liquefaction was effectively reduced by increasing D_{50} appropriately.

Yoshimi and Oh-oka (1975) and Lee and Focht (1975) confirmed that the vibration frequency had small influence on liquefaction strength in generation seismic frequency range. The result was verified by Zhang and Wang (1990) with vibration frequency from 1 to 20 Hz. However, Guo

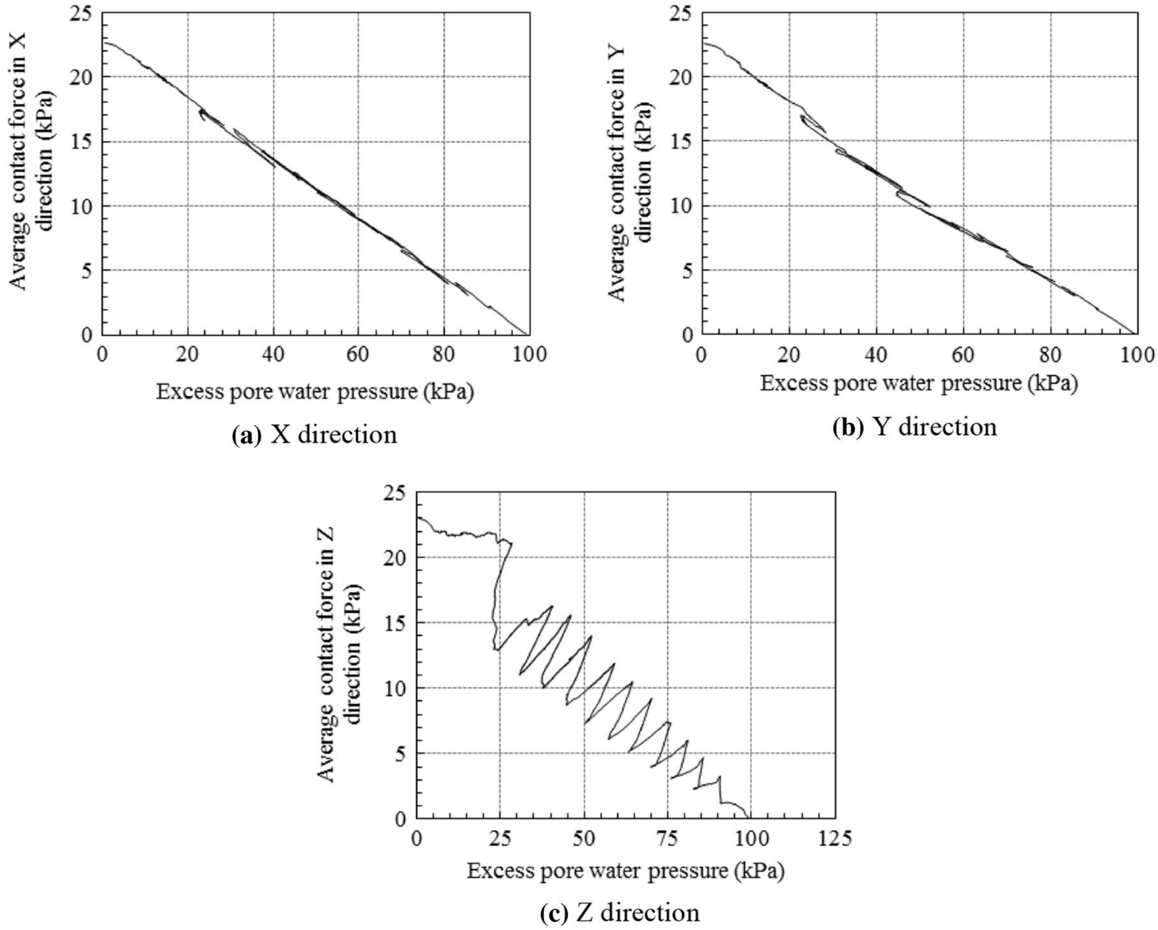

Fig. 13 Excess pore water pressure-average contact force curves of numerical simulation

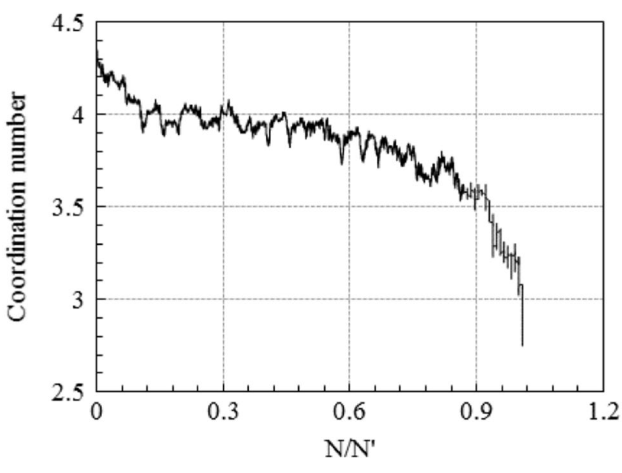

Fig. 14 Coordination number and *N*/*N*′ curve

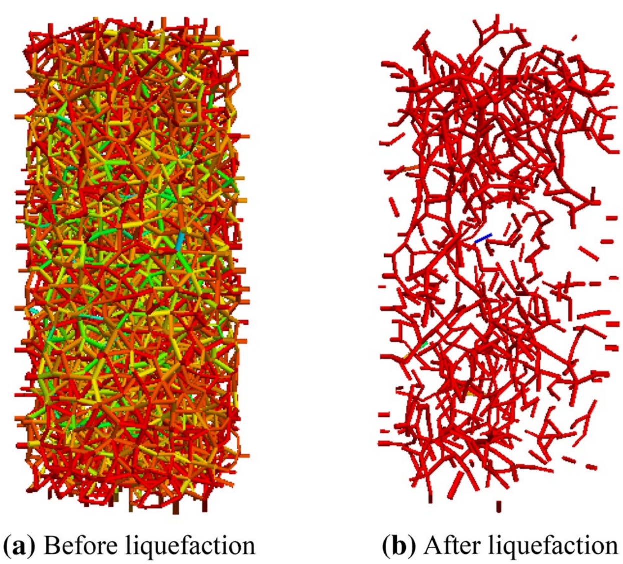

Fig. 15 Contact force chain between the particles of numerical sample

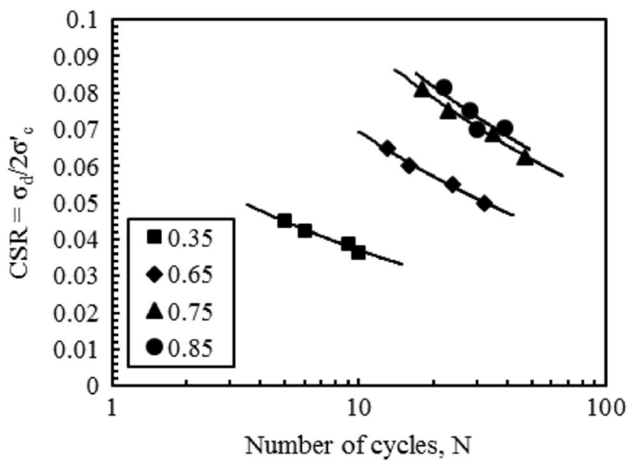

Fig. 16 CSR and N curve of different D_{50}

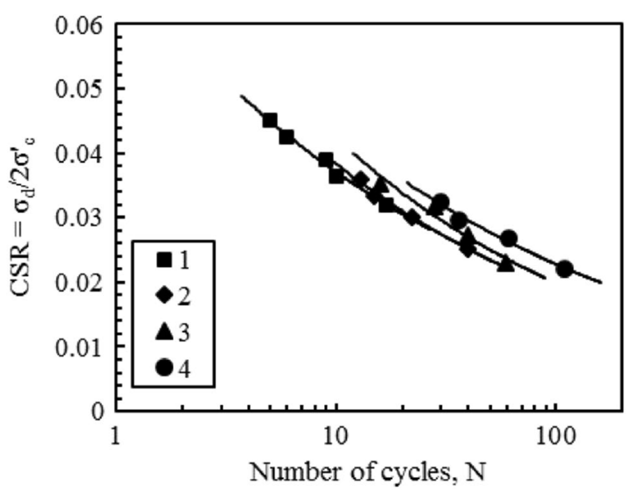

Fig. 17 CSR and N curve of different loading frequencies

and He (2009) observed that the CSR of saturated loose and dense sands increased with the increase of vibration frequency. In this study, nearly no change was observed in CSR when the vibration frequency was between 1 and 2 Hz. CSR slightly increased with the increase of vibration frequency from 2 to 4 Hz (Fig. 17). CSR increased by approximately 8% when the frequency increased at a step of 1 Hz. The effect of a wide frequency on liquefaction should be investigated.

Combined countermeasures for improving liquefaction resistance

According to Zhou et al. (2011) and Yang et al. (2012), liquefaction resistance and pore water pressure of saturated sands were significantly influenced by silty interlayer under cyclic loading. To investigate the effect of different layer combinations, FS, CS, FS–CS combination, and CS–FS–CS combination models were established to investigate the liquefaction resistance of the combined layers. The particle radii of FS and CS were 0.2–0.5 and 0.5–0.8 mm in the numerical models, respectively. The numerical models are presented in Fig. 18. The effect of different layer combinations on CSR with the number of cycles N required to reach the liquefaction is shown in Fig. 19. The CS layer had the largest CSR, and the FS layer was the most susceptible to liquefaction. The CS–FS and CS–FS–CS combination layers showed greater CSR than the FS layer. Therefore, the liquefaction resistance of dredged silty-FS was improved by properly combining FS and CS during the dredging course of land reclamation.

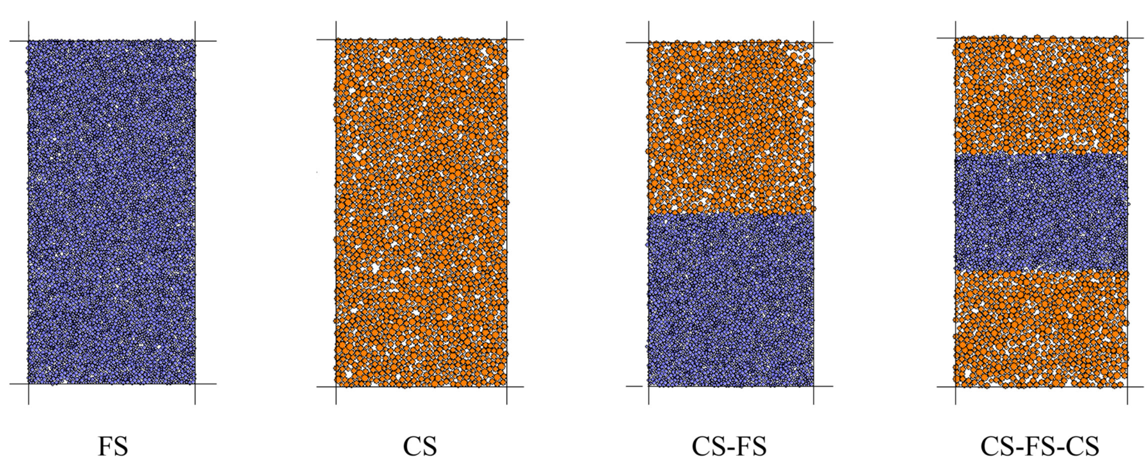

Fig. 18 Numerical models of layer combinations (orange represents FS, and blue represents CS)

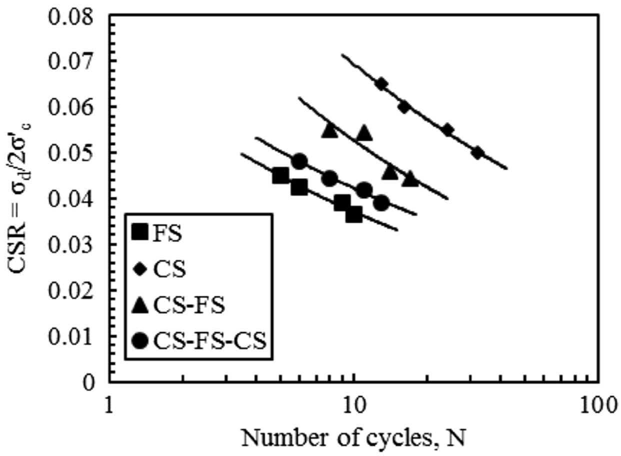

Fig. 19 CSR and *N* curve of different layer combinations

Conclusions

In this study, cyclic triaxial tests and PFC simulations were performed to investigate the influencing factors and microscopic mechanism of liquefaction for dredged silty-FS. The conclusions are as follows:

1. On the basis of cyclic tests, CSR decreased with the increase of f_s from 0 to 18% and sharply decreased by approximately 22% when f_s value was greater than 6%. CSR first decreased with the increase of f_c up to a threshold value of 12% and increased with the increase of f_c. CSR increased with the increase of f_{ird} from 52 to 92% and f_{csr} from 1 to 2 and decreased with the increase of f_{cs} from 50 to 300 kPa.
2. The effects of f_{ird} and f_{csr} on CRR_{30} were positive, and the effects of f_s and f_{cs} on CRR_{30} were negative. CRR $_{30}$ first decreased and reached a minimum at a threshold clay content of approximately $f_c = 12\%$ and increased with the increase of f_c. The effect of single factor on CRR_{30} was sorted as $f_s > f_{cs} > f_c$ and $f_{ird} > f_{csr}$.
3. The regression model was proposed to represent the effects of f_s, f_{cs}, f_c, f_{ird}, and f_{csr} on CRR_{30}, and response surface methodology was employed to analyze the mutual influence among five independent variables.
4. Internal fabric changes in liquefaction were simulated using PFC. The average microscopic contact force and coordination number between the particles controlled the macroscopic mechanical behavior of sands. Sand liquefaction was due to the cumulative loss of coordination number under cyclic loading.
5. On the basis of numerical tests, CSR increased with the increase of D_{50} and vibration frequency. The influence of vibration frequency was relatively small. In addition, the CS–FS and CS–FS–CS combination layers showed greater liquefaction resistance than the FS layer. In the filling process, the interbed of FS and CS improved the liquefaction resistance of dredged silty-FS to a certain extent.

Acknowledgements This work is sponsored by the research of National Key Basic Research Program of China (2014CB046901), Shanghai Pujiang Program (15PJD039), Science and Technology Commission of Shanghai Municipality (16DZ1201303), CCCC Key Lab of Environment Protection & Safety in Foundation Engineering of Transportation, Key Laboratory of Karst Collapse Prevention CAGS, Opening fund of State Key Laboratory of Geohazard Prevention and Geoenvironment Protection (Chengdu University of Technology) (SKLGP2018K019), National Key R&D Program of China (2017YFC0806000), JG Training Fund for Key Defense Research Project from Tongji University, GDUE Open Funding (SKLGDUEK1417), Shanghai Institute of Geological Survey [2016(D)-008(F), 2017(D)-005(F)-02], LSMP Open Funding (KLLSMP201403, KLLSMP201404), Consulting Research Project of Chinese Academy of Engineering (2016-XY-51), the National Natural Science Foundation of China (No. 41072205) and Key Discipline Construction Program of Shanghai (Geological Engineering, No. B308).

References

Amini F, Qi GZ (2000) Liquefaction testing of stratified silty sands. J Geotech Geoenviron Eng Proc ASCE 126:208–217

Arab A, Sadek M, Belkhatir M, Shahrour I (2014) Monotonic preloading effect on the liquefaction resistance of chlef silty sand: a laboratory study. Arab J Sci Eng 39:685–694

Baziar MH, Sharafi H (2011) Assessment of silty sand liquefaction potential using hollow torsional tests—an energy approach. Soil Dyn Earthq Eng 31:857–858

Belkhatir M, Arab A, Della N, Missoum H, Schanz T (2010) Liquefaction resistance of Chlef river silty sand: effect of low plastic fines and other parameters. Acta Polytech Hung 7:119–137

Belkhatir M, Arab A, Schanz T, Missoum H, Della N (2011) Laboratory study on the liquefaction resistance of sand-silt mixtures: effect of grading characteristics. Granul Matter 13:599–609

Belkhatir M, Arab A, Della N, Schanz T (2014(B) Laboratory study on the hydraulic conductivity and pore pressure of sand–silt mixtures. Mar Georesour Geotechnol 32:106–122

Bouckovalas GD, Andrianopoulos KI, Papadimitriou AG (2003) A critical state interpretation for the cyclic liquefaction resistance of silty sands. Soil Dyn Earthq Eng 23:115–125

Cundall PA, Strack ODL (1979) A discrete numerical model for granular assemblies. Geotechnique 29:47–65

Dobry R, Abdoun T, Stokoe IIKH., Moss RES, Hatton M, Ganainy HE (2015) Liquefaction potential of recent fills versus natural sands located in high-seismicity regions using shear-wave velocity. J Geotech Geoenviron Eng 141:04014112

El-Sekelly W, Dobry R, Abdoun T, Steidl JH (2016) Centrifuge modeling of the effect of preshaking on the liquefaction resistance of silty sand deposits. J Geotech Geoenviron Eng 142:04016012

Finn WD, Pickering DJ, Bransby PL (1971) Sand liquefaction in triaxial and simple shear tests. J Geotech Eng Div ASCE 97:639–660

Guo Y, He L (2009) The influences of the vibration frequencies on liquefaction strength of saturated sands. J Disaster Prev Mitig Eng 29(6):618–623 **(in Chinese)**

Huang Y, Wang L (2016) Laboratory investigation of liquefaction mitigation in silty sand using nanoparticles. Eng Geol 204:23–32

Ishihara K (1993) Liquefaction and flow failure during earthquakes. Geotechnique 43:351–415
Ishihara K, Tatsuka K, Yasuda S (1975) Undrained deformation and liquefaction of sand under cyclic stresses. Soils Found 15:29–44
Jafarian Y, Vakili R, Abdollahi AS (2013) Prediction of cyclic resistance ratio for silty sands and its applications in the simplified liquefaction analysis. Comput Geotech 52:54–62
Karim ME, Alam MJ (2014) Effect of non-plastic silt content on the liquefaction behavior of sand–silt mixture. Soil Dyn Earthq Eng 65:142–150
Kim J, Kawai T, Kazama M, Mori T (2016) Density index for estimating the post liquefaction volumetric strain of silty soils. Int J Geomech 16:C4015005
Koester JP (1994) Liquefaction characteristics of silt: ground failures under seismic condition. Geotech Spec Publ ASCE 44:105–116
Lade PV, Yamamuro JA (1997) Effects of non-plastic fines on static liquefaction of sands. Can Geotech J 34:918–928
Lee KL, Focht JA (1975) Cyclic testing of soil for ocean wave loading problems, 7th annual offshore technology conference, Houston, Texas
Lee WF, Ishihara K, Chen CC (2012) Liquefaction of silty sand preliminary studies from recent Taiwan, New Zealand, and Japan earthquakes. Proceedings of the international symposium on engineering lessons learned from the 2011 Great East Japan Earthquake, March 1–4, 2012, Tokyo, Japan
Liu HL, Yu XJ (1999) Advance in soil dynamics and geotechnical earthquake engineering. J Hohai Univ 27:6–15 **(in Chinese)**
Liu Y, Zhou J, Wu SC (2007a) Micro-numerical simulation of cyclic biaxial test I: results of loose sand. Chin J Geotech Eng 29:1035–1041 **(in Chinese)**
Liu Y, Wu SC, Zhou J (2007b) Micro-numerical simulation of cyclic biaxial test II: results of dense sand. Chin J Geotech Eng 29:1676–1682 **(in Chinese)**
Monkul MM, Yamamuro JA (2011) Influence of silt size and content on liquefaction behavior of sands. Can Geotech J 48:931–942
Monkul MM, Gültekin C, Gülver M, Akın Ö, Eseller-Bayat E (2015) Estimation of liquefaction potential from dry and saturated sandy soils under drained constant volume cyclic simple shear loading. Soil Dyn Earthq Eng 75:27–36
Ng TT, Dobry R (1994) Numerical simulations of monotonic and cyclic loading of granular soil. J Geotech Eng 120:388–403
Papadopoulou A, Tika T (2008) The effect of fines on critical state and liquefaction resistance characteristics of nonplastic silty sands. Soils Found 48:713–725
Park SS, Kim YS (2013) Liquefaction resistance of sands containing plastic fines with different plasticity. J Geotech Geoenviron Eng 139:825–830
Polito CP (1999) The effects of non-plastic and plastic fines on the liquefaction of sandy soils. [Ph.D. Thesis], Virginia Polytechnic Institute and State University, Virginia
Polito CP, Martin JR (2001) Effects of nonplastic fines on the liquefaction resistance of sands. J Geotech Geoenviron Eng 127:408–415
Rahman MM, Baki MAL, Lo SR (2014) Prediction of undrained monotonic and cyclic liquefaction behavior of sand with fines based on the equivalent granular state parameter. Int J Geomech 14:254–266
Ravishankar BV (2006) Cyclic and monotonic undrained behavior of sandy soils [Ph.D. thesis]. Indian Institute of Science, Bangalore in the Faculty of Engineering
Sadrekarimi A (2013) Influence of fines content on liquefied strength of silty sands. Soil Dyn Earthq Eng 55:108–119
Seed HB, Lee KL (1966) Liquefaction of saturated sands during cyclic loading. J Soil Mech Found Div 92:105–134
Sitharam TG (2003) Discrete element modeling of cyclic behavior of granular materials. Geotech Geol Eng 21:297–329
Sitharam TG, Vinod JS (2009) Critical state behavior of granular materials from isotropic and rebounded paths: DEM simulations. Granul Matter 11:33–42
Stamatopoulos CA (2010) An experimental study of the liquefaction strength of silty sands in terms of the state parameter. Soil Dyn Earthq Eng 30:662–678
Stamatopoulos CA, Lopez-Caballero F, Modaressi-Farahmand-Razavi A (2015) The effect of preloading on the liquefaction cyclic strength of mixtures of sand and silt. Soil Dyn Earthq Eng 78:189–200
Taiba AC, Belkhatir M, Kadri A, Mahmoudi Y, Schanz T (2016) Insight into the effect of granulometric characteristics on the static liquefaction susceptibility of silty sand soils. Geotech Geol Eng 34:367–382
Takch AE, Sadrekarim A, Naggar EN (2016) Cyclic resistance and liquefaction behavior of silt and sandy silt soils. Soil Dyn Earthq Eng 83:98–109
Thevanayagam S, Martin GR (2002) Liquefaction in silty soils-screening and remediation issues. J Soil Dyn Earthq Eng 22:1035–1042
Ueng TS, Sun CW, Chen CW (2004) Definition of fines and liquefaction resistance of Maoluo river soil. Soil Dyn Earthq Eng 24:745–775
Wang XH, Zhou HL (2001) Effect of the consolidation ratio on saturated sand liquefaction. China Railway Science 22:121–126 **(in Chinese)**
Xenaki VC, Athanasopoulos GA (2003) Liquefaction resistance of sand–silt mixtures: an experimental investigation of the effect of fines. Soil Dyn Earthq Eng 23:183–194
Yang YX, Hu JH, Jia MC, Huang ZQ (2012) Effects of silty interlayer on liquefaction characteristics saturated stratified sands. Chin J Undergr Space Eng 8(6):1215–1220 **(in Chinese)**
Yassine B, Ali B, Jean C, Jean-Claude D (2015) Liquefaction susceptibility study of sandy soils: effect of low plastic fines. Arab J Geosci 8:605–618
Yilmaz Y, Mollamahmutoglu M (2009) Characterization of liquefaction susceptibility of sands by means of extreme void ratios and/or void ratio range. J Geotech Geoenviron Eng 135:1986–1990
Yoshimi Y, Oh-oka H (1975) Influence of degree of shear stress reversal on the liquefaction potential of saturated sand. Soils Foundations 15(3):27–40
Zhang JM, Wang WX (1990) Influence of vibration frequency on dynamic characteristics of saturated sand. Chin J Geotech Eng 12(1):89–97 **(in Chinese)**
Zhou J, Chi Y (2003) Mesomechanical simulation of sand mechanical properties. Rock Soil Mech 24:901–906 **(in Chinese)**
Zhou J, Chi Y, Chi YW (2000) The method of particle flow coed and PFC^{2D} code. Rock Soil Mech 21:271–274 **(in Chinese)**
Zhou J, Yang YX, Liu Y (2009) Numerical modeling of sand liquefaction behavior under cyclic loading. Rock Soil Mech 30:1083–1088 **(in Chinese)**
Zhou J, Chen XL, Yang YX, Jia MC (2011) Study of liquefaction characteristics of saturated sands by dynamic triaxial test. Rock Soil Mech 32(4):967–978 **(in Chinese)**